Geophysical Research Letters

RESEARCH LETTER
10.1029/2020GL089933

Arctic Amplification: A Rapid Response to Radiative Forcing

Michael Previdi[1], Tyler P. Janoski[1,2], Gabriel Chiodo[3,4], Karen L. Smith[1,5], and Lorenzo M. Polvani[1,2,4]

[1]Lamont-Doherty Earth Observatory, Columbia University, Palisades, NY, USA, [2]Department of Earth and Environmental Sciences, Columbia University, New York, NY, USA, [3]Institute for Atmospheric and Climate Science, Swiss Federal Institute of Technology Zürich, Zürich, Switzerland, [4]Department of Applied Physics and Applied Mathematics, Columbia University, New York, NY, USA, [5]Department of Physical and Environmental Sciences, University of Toronto, Scarborough, Toronto, Ontario, Canada

Key Points:
- Arctic amplification develops rapidly (within a few months) in climate models forced with abrupt CO_2 quadrupling
- This rapid response is produced by a positive lapse rate feedback over the Arctic
- The response occurs before Arctic sea ice loss becomes significant

Supporting Information:
- Supporting Information S1

Correspondence to:
M. Previdi,
mprevidi@ldeo.columbia.edu

Citation:
Previdi, M., Janoski, T. P., Chiodo, G., Smith, K. L., & Polvani, L. M. (2020). Arctic amplification: A rapid response to radiative forcing. *Geophysical Research Letters*, *47*, e2020GL089933. https://doi.org/10.1029/2020GL089933

Received 21 JUL 2020
Accepted 17 AUG 2020
Accepted article online 25 AUG 2020

Abstract Arctic amplification (AA) of surface warming is a prominent feature of anthropogenic climate change with important implications for human and natural systems. Despite its importance, the underlying causes of AA are not fully understood. Here, analyzing coupled climate model simulations, we show that AA develops rapidly (within the first few months) following an instantaneous quadrupling of atmospheric CO_2. This rapid AA response—which occurs before any significant loss of Arctic sea ice—is produced by a positive lapse rate feedback over the Arctic. Sea ice loss is therefore not needed to produce polar-amplified warming, although it contributes significantly to this warming after the first few months. Our results provide new and compelling evidence that AA owes its existence, fundamentally, to fast atmospheric processes.

Plain Language Summary Climate warming is greater in the Arctic than at lower latitudes, a phenomenon known as Arctic amplification. Despite its importance for humans and ecosystems, the causes of Arctic amplification are not fully understood. Sea ice loss has long been thought to be a primary cause. However, we show here that Arctic amplification happens faster than sea ice loss in climate models when atmospheric CO_2 is increased. This indicates that atmospheric processes alone are capable of causing Arctic amplification.

1. Introduction

One of the prominent features of recent climate change is an enhancement of near-surface warming over the Arctic, referred to as Arctic amplification (AA). This enhanced warming relative to lower latitudes has had and will have important impacts on a range of human and natural systems, both within and outside the Arctic (Osborne et al., 2018; SWIPA, 2017). Thus, understanding its causes is critical for developing robust climate model projections and preparing for the consequences of global change. AA has long been attributed to the retreat of sea ice and snow cover at high northern latitudes (Dai et al., 2019; Hall, 2004; Manabe & Stouffer, 1980), which acts as a positive feedback on climate warming by increasing the surface absorption of shortwave radiation and the exchange of heat between the ocean and atmosphere. The importance of other processes has also been highlighted, however. These include temperature feedbacks that affect the emission of longwave radiation (Pithan & Mauritsen, 2014) and changes in poleward heat transport by the atmosphere (Cai, 2005; Graversen & Langen, 2019) and ocean (Marshall et al., 2015; Singh et al., 2017). These physical processes operate on very different timescales. Thus, examining the timescales of AA can provide insight into which processes are most important to its existence.

We here examine AA timescales using climate model simulations from the fifth Coupled Model Intercomparison Project (CMIP5) that were forced with an instantaneous quadrupling of atmospheric CO_2 ($4\times CO_2$). Additional details about the CMIP5 data are provided in section 2. In section 3, we assess the timescales of AA in CMIP5 simulations. We show that AA develops very rapidly (within the first few months) following $4\times CO_2$, and we evaluate changes to the top-of-atmosphere (TOA) energy budget in order to understand this response. Conclusions from our analysis are presented in section 4.

2. Data and Methods

2.1. CMIP5 Data

We analyze simulations from the following 21 global coupled climate models that were included in CMIP5: ACCESS1-0, ACCESS1-3, bcc-csm1-1, BNU-ESM, CanESM2, CCSM4, CNRM-CM5, CSIRO-Mk3-6-0, FGOALS-g2, FGOALS-s2, GFDL-CM3, GFDL-ESM 2G, inmcm4, IPSL-CM5A-LR, IPSL-CM5B-LR, MIROC5, MIROC-ESM, MPI-ESM-LR, MPI-ESM-P, MRI-CGCM3, and NorESM1-M. These models were selected because they provided all of the necessary output for our energy budget analysis (see section 2.2). For each model, we analyzed the following monthly mean atmospheric fields: surface (skin) temperature, surface pressure, surface air temperature (SAT), air temperature and specific humidity, zonal and meridional wind components, TOA radiative energy fluxes (all-sky and clear-sky), and surface energy fluxes. Additionally, we examined two monthly mean ocean fields (seawater potential temperature and the net surface heat flux) and one monthly sea ice field (sea ice concentration).

For each model, these fields were obtained for two different CMIP5 experiments (Taylor et al., 2012): a control experiment with constant preindustrial boundary conditions (piControl) and a forced experiment (initialized from piControl) in which the atmospheric CO_2 concentration was instantaneously quadrupled (abrupt4×CO_2). A single ensemble member (r1i1p1) is used from each model for each of these experiments.

We compute responses to 4×CO_2 as the difference between the forced experiment and the monthly climatology of the control experiment (i.e., abrupt4×CO_2 minus piControl). The monthly climatology is based on the last 50 years of piControl. For reference, the total length of the abrupt4×CO_2 simulations is ~150 years, and the piControl simulations range in length from 430 to over 1,000 years.

2.2. Energy Budget Analysis

The perturbation energy budget of a column extending from the TOA to the base of the ocean mixed layer (ML) can be written as follows:

$$\Delta H = \Delta R + \Delta AHT + \Delta OHT \tag{1}$$

where H is the net heating of the column, R is the net downward TOA radiation, AHT is the convergence of the atmospheric heat transport, OHT is the convergence of the ocean heat transport within the ML, and Δ denotes the response to 4×CO_2. We quantify the terms on the right-hand side of Equation 1 in order to gain insight into the physical processes driving warming in the CMIP5 simulations.

The TOA radiation response ΔR is decomposed as follows:

$$\Delta R = \Delta R_{CO2} + \Delta R_T + \Delta R_{WV} + \Delta R_{Albedo} + \Delta R_{Cloud} \tag{2}$$

where ΔR_{CO2} is the 4×CO_2 radiative forcing. The remaining terms on the right-hand side of Equation 2 represent feedbacks due to the responses of surface and tropospheric temperatures (ΔR_T), tropospheric water vapor (ΔR_{WV}), surface albedo (ΔR_{Albedo}), and clouds (ΔR_{Cloud}). The temperature feedback is further decomposed as follows:

$$\Delta R_T = \Delta R_P + \Delta R_{LR} \tag{3}$$

where ΔR_P is the Planck response representing the TOA radiation change due to vertically uniform warming and ΔR_{LR} is the tropospheric lapse rate feedback. Following previous studies (Goosse et al., 2018; Pithan & Mauritsen, 2014), we express the Planck response as a local deviation from the global mean:

$$\Delta R_{P'} = \Delta R_P - \Delta R_{\bar{P}} \tag{4}$$

where the prime and overbar denote the local deviation and global mean, respectively.

The 4×CO_2 radiative forcing was not available for the CMIP5 models used in our analysis. We therefore computed ΔR_{CO2} using the Parallel Offline Radiative Transfer (PORT) model (Conley et al., 2013). Our estimate of the CO_2 forcing includes the effect of stratospheric temperature adjustment, which is calculated in PORT assuming fixed dynamical heating (Fels et al., 1980; Ramanathan & Dickinson, 1979). To compute the

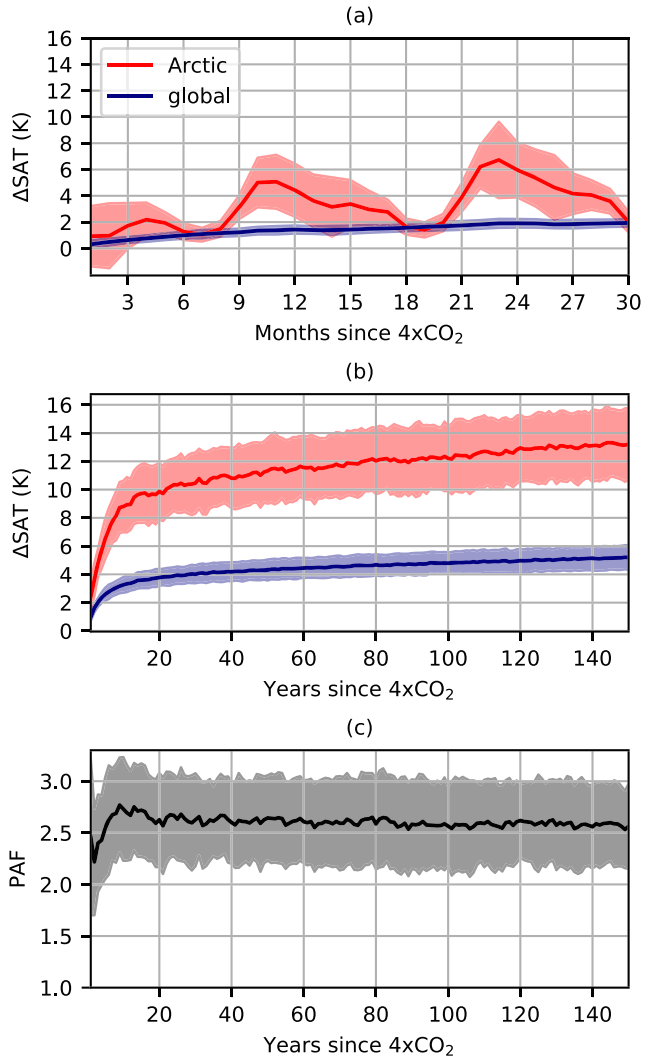

Figure 1. (a) Monthly Arctic (70–90°N) and global SAT response for the first 30 months following 4×CO_2 in the CMIP5 simulations. Lines indicate the multimodel mean and shading the ±1-sigma spread. (b) As in (a) but showing the annual SAT response for the entire 150 years of the simulations. (c) Annual mean polar amplification factor (PAF) in the CMIP5 simulations. The PAF is defined as the ratio of Arctic (70–90°N) to global SAT response. The line indicates the multimodel mean PAF, and shading denotes the ±1-sigma spread.

remaining terms on the right-hand side of Equation 2, we employ the radiative kernel technique (Soden et al., 2008), using kernels from Version 5 of the Community Atmosphere Model (Pendergrass & Conley, 2018). For ΔR_{Cloud}, we use the kernels to adjust the CMIP5 cloud radiative effect response to account for the responses of the noncloud variables (Soden et al., 2008).

The AHT convergence is calculated as a residual in the atmospheric column energy budget:

$$AHT = \frac{dE}{dt} - R + R_{SFC} \tag{5}$$

where dE/dt is the time rate of change of the atmospheric energy storage and R_{SFC} is the net downward surface energy flux (on the models' atmospheric grid). Similarly, we compute the OHT convergence as a residual in the ML energy budget:

$$OHT = \frac{dOHC_{ML}}{dt} - F_{SFC} \tag{6}$$

where $dOHC_{ML}/dt$ is the time rate of change of the ocean heat content (OHC) in the ML and F_{SFC} is the net downward surface heat flux into the liquid water column (on the models' ocean grid). We define the ML depth as the shallowest depth at which the temperature differs from the surface temperature by at least 0.2 K (Carton et al., 2018).

All of the terms in the above equations are calculated on a grid point basis and are spatially averaged (using area weighting) to form Arctic (70–90°N) and global means. Terms are expressed as warming contributions (Goosse et al., 2018; Pithan & Mauritsen, 2014) by normalizing the energy flux responses (in W m^{-2}) by the magnitude of the global mean Planck response (3.2 W m^{-2} K^{-1}).

3. Results

3.1. AA as a Rapid Response to CO_2 Forcing

We begin by considering the time evolution of the Arctic (70–90°N) and global mean SAT in the initial months following 4×CO_2 (Figure 1a). AA is clearly evident within the first few months. For instance, averaged over Months 1–3 (January–March), the multimodel mean Arctic SAT response (1.2 K) is already significantly greater than the global SAT response (0.5 K) based on a t test ($p < 0.05$). This remains the case through the rest of the spring (Months 4 and 5). However, during summer (Months 6–8), Arctic and global SAT responses are very similar, indicating that AA has essentially disappeared. It reappears prominently in the fall though, with a peak during October and November (Months 10 and 11). Similar seasonal variability in AA is evident in the second year following 4×CO_2 (Months 13–24). This seasonal variability is qualitatively consistent with that seen previously in model simulations (Lu & Cai, 2009) and in observations (Serreze et al., 2009).

It is useful to compare the time evolution of AA in these initial months with the time evolution of Arctic sea ice (Figure 2). Sea ice loss is insignificant in the first few months following 4×CO_2, with a decrease in total sea ice area (SIA) of only ~1–2% in Months 1–3. This suggests that ice loss is unlikely to contribute significantly to AA during these first few months. In contrast, SIA decreases become considerable after the first few months, reaching ~20% at the end of the first melt season (Month 9) and ~35% at the end of the second melt season (Month 21). Thus, significant sea ice loss during fall—and associated increases in ocean-to-atmosphere heat flux (e.g., Bintanja & van der Linden, 2013; Boeke & Taylor, 2018; Dai et al., 2019; Kim

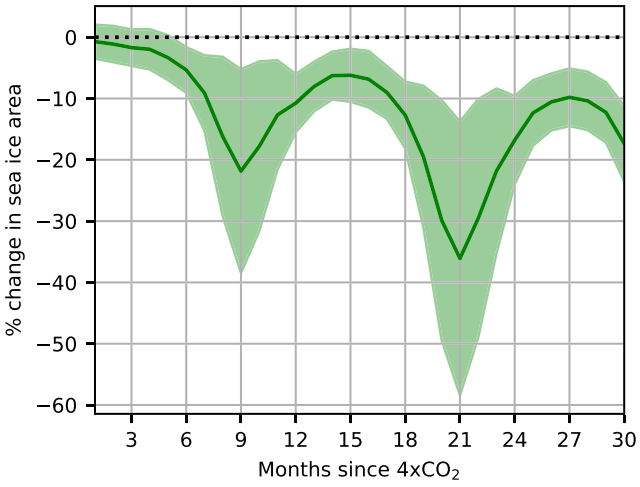

Figure 2. Relative response of the Northern Hemisphere total sea ice area in the first 30 months following 4×CO_2. The line indicates the multimodel mean, and shading denotes the ±1-sigma spread.

et al., 2016; Screen & Simmonds, 2010a, 2010b)—likely contribute to the peak in AA during this season (Figure 1a).

We now consider the time evolution of the Arctic and global SAT on longer timescales (Figure 1b). Both quantities increase rapidly during the first decade or so of the model simulations, followed by a more gradual increase thereafter. This warming occurs at proportionately the same rate over the Arctic and the planet as a whole, leading to a nearly constant PAF (polar amplification factor, defined as the ratio of Arctic to global SAT response) of just over 2.5, but with some variability during the early years of the simulations (Figure 1c). The warming occurring during the first decade is associated with an adjustment of the ocean ML to the imposed CO_2 forcing. Over ensuing decades, warming occurs more gradually as the deep ocean comes into equilibrium. The time evolution of surface warming in the CMIP5 simulations that is documented here is qualitatively similar to the one seen in earlier modeling studies (Hansen et al., 2011; Marshall et al., 2015) that examined the response to an abrupt change in greenhouse gas forcing.

We next examine the spatial structure of model-simulated warming. Figure 3a shows a latitude-pressure (or height) plot of the air temperature response averaged over the first 3 months (January–March) of the model simulations. An AA pattern is already evident within these first few months, with lower tropospheric warming over the Arctic that is markedly stronger than that at lower latitudes. The maximum near-surface warming occurs between 65°N and 70°N and is associated with the rapid warming of high-latitude land areas (supporting information Figure S1). The vertical structure of the simulated Arctic warming—with the maximum warming concentrated near the surface—is a characteristic feature of AA. This vertical structure has long been linked to the strong static stability of the Arctic boundary layer (Manabe & Stouffer, 1980; Manabe & Wetherald, 1975), which limits vertical mixing and thus largely confines surface heating anomalies to the lowest layers of the atmosphere.

When we consider the temperature response averaged over the first year, we see that the maximum near-surface warming has shifted northward and now lies between 80°N and 90°N (Figure 3b). This northward shift is likely a response to sea ice loss that has already become significant within the first year

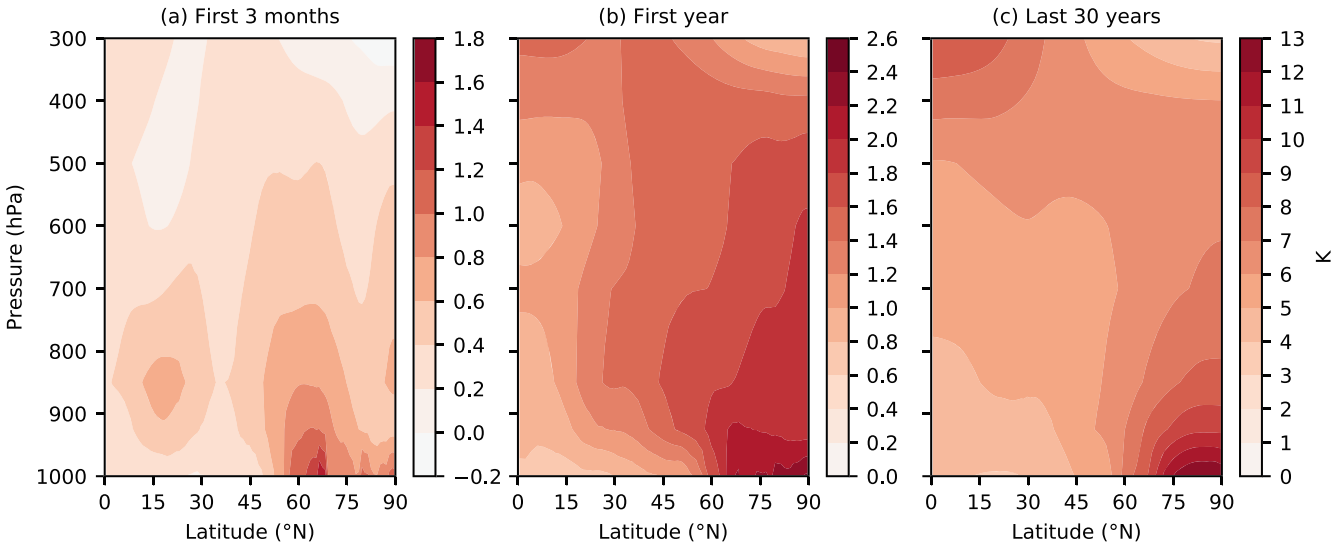

Figure 3. Latitude-pressure plots of the multimodel mean air temperature response averaged over (a) the first 3 months (January–March), (b) the first year, and (c) the last 30 years of the CMIP5 simulations.

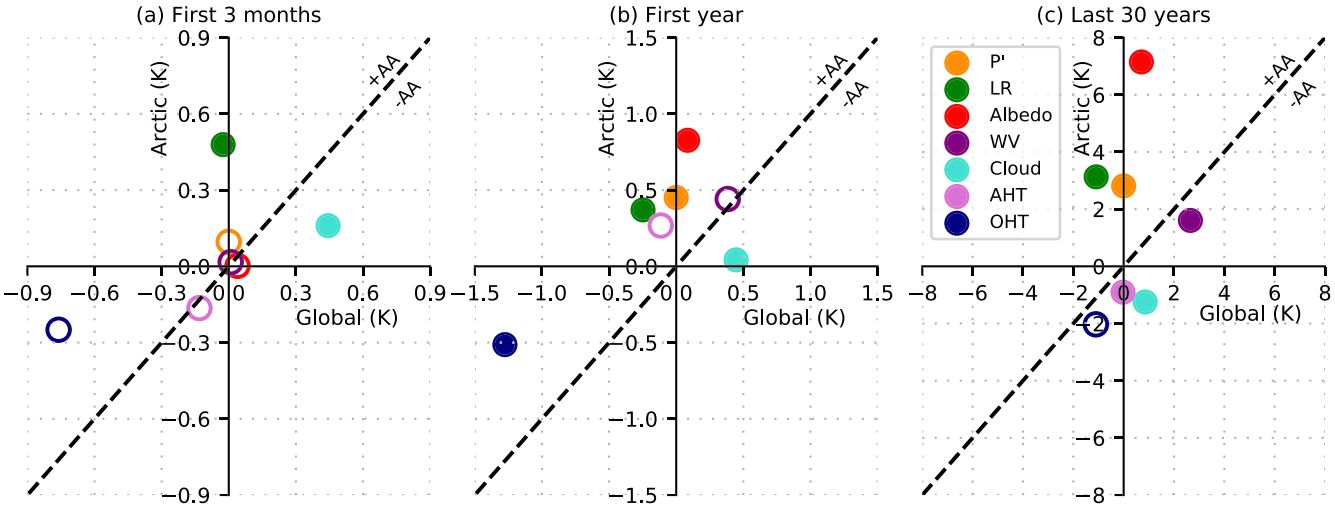

Figure 4. Multimodel mean Arctic and global warming contributions from feedbacks and energy transport responses (see section 2.2) for (a) the first 3 months (January–March), (b) the first year, and (c) the last 30 years of the CMIP5 simulations. Filled (empty) circles indicate that the Arctic minus global warming contribution is (is not) significantly different from zero at the 95% level based on a *t* test.

(Figure 2). The temperature response in the first year also exhibits tropically amplified warming in the upper troposphere that is not present (or at least is much weaker) in the first 3 months. Such tropically amplified warming is known to result from increases in tropical convective heating, which are closely tied to tropical sea surface temperature (SST) increases (Stocker et al., 2013). Thus, the absence of this feature in the first 3 months of the model simulations can be explained by the fact that tropical SST responses are minimal during this time (not shown). Finally, we note that the basic pattern of warming established in the first year (Figure 3b) is similar to the one seen in the last 30 years of the simulations (Figure 3c). However, the magnitude of warming is much larger in the latter case (e.g., ~10 K larger in the Arctic lower troposphere).

3.2. Causes of Model-Simulated Warming

We now examine TOA energy budget responses in order to gain insight into the physical causes of AA (see section 2.2). The first response to consider is the direct radiative forcing from the quadrupling of CO_2 (Figure S2). CO_2 forcing is largest at low latitudes and decreases toward the poles. This meridional structure has been documented previously (Hansen et al., 1997) and is due to decreases in the climatological surface temperature and tropospheric vertical temperature gradient with latitude (Merlis, 2015; Smith et al., 2018; Zhang & Huang, 2014), leading to the strongest enhancement of the greenhouse effect at low latitudes when CO_2 is increased. Therefore, from the perspective of the TOA energy budget, direct CO_2 forcing opposes AA by preferentially warming the tropics. This suggests that other changes to the energy budget occurring in response to the CO_2 forcing are needed to explain the model-simulated AA.

We evaluate these energy budget responses for the same three time periods considered above: the first 3 months, the first year, and the last 30 years of the $4\times CO_2$ simulations (Figure 4). In the first 3 months (Figure 4a), the tropospheric lapse rate feedback is positive over the Arctic but close to zero in the global mean. Thus, the lapse rate feedback strongly contributes to the rapid AA response. In contrast, cloud feedback opposes AA, since it is more positive in the global mean than over the Arctic. All remaining energy budget responses make insignificant contributions to the multimodel mean AA in the first 3 months (denoted by empty circles in Figure 4a). In essence, this means either that the multimodel mean contributions are small and/or that individual models disagree on the sign of the contribution (i.e., contributing to or opposing AA; see Figure S3).

In the first year of the model simulations (Figure 4b), the lapse rate feedback contributes to AA and the cloud feedback opposes AA, as in the first 3 months. Additional positive contributions to AA in the first year come from the surface albedo feedback (which makes the largest contribution), the Planck response, and the OHT convergence response. When we consider instead the last 30 years of the simulations (Figure 4c), we see that

the temperature (Planck and lapse rate) and surface albedo feedbacks still contribute significantly to AA. This is in agreement with previous studies (Goosse et al., 2018; Pithan & Mauritsen, 2014) that examined the long-term response to 4×CO_2 in CMIP5 models. We find negative contributions to AA in the last 30 years from cloud and water vapor feedbacks, also confirming these previous studies. Additionally, decreases in AHT into the Arctic oppose AA in the last 30 years. AHT decreases are consistent with reductions in the meridional temperature gradient due to polar-amplified warming (Hwang et al., 2011).

Given the importance of the temperature and surface albedo feedbacks for AA, it is worth discussing their physical meaning in a bit more detail. As noted in section 2.2, the total temperature feedback can be decomposed into contributions from vertically uniform warming (Planck response) and the tropospheric lapse rate response. The Planck response is weaker over the colder Arctic relative to the global mean—meaning a smaller increase in outgoing longwave radiation (OLR) per degree of warming—which contributes to AA. Globally averaged, the tropospheric lapse rate response is characterized by a reduction in the rate of temperature decrease with height (i.e., increased static stability), largely reflecting moist adiabatic adjustment to surface warming in the tropics (Manabe & Wetherald, 1975). Such a response of the temperature profile leads to a larger increase in OLR than would occur from the Planck response alone, representing a negative feedback on surface warming. However, the opposite occurs over the Arctic where there is a decrease in static stability associated with a weakening of the climatological near-surface inversion (Bintanja et al., 2012). This opposes the basic Planck response and represents a positive feedback on surface warming. Thus, both the Planck and lapse rate components of the temperature feedback contribute to AA, as shown in our analysis of the CMIP5 models. The other main contribution to AA in the first year (Figure 4b) and in the last 30 years (Figure 4c) of the model simulations comes from surface albedo feedback. This feedback is associated with the loss of snow cover and sea ice, which preferentially warms the Arctic region by increasing the surface absorption of shortwave radiation. Note that the surface albedo feedback over the Arctic is negligible in the first 3 months (January–March; see Figure 4a), which is expected since insolation over the polar cap is minimal during this time.

4. Conclusions

We have demonstrated here that AA is a rapid response to radiative forcing, occurring within the first few months after CO_2 is instantaneously quadrupled in CMIP5 climate models. This rapid AA response was found to be caused by a positive tropospheric lapse rate feedback over the Arctic. The notion of AA as a rapid response is supported by the recent finding that the rapid adjustment of the atmospheric temperature field to CO_2 forcing is characterized by polar-amplified warming in the lower troposphere (Wang & Huang, 2020). In this view, fast atmospheric processes act to establish AA before any significant responses of the ocean and sea ice can occur. Accordingly, we find that Arctic sea ice loss is insignificant in the first few months following 4×CO_2, suggesting that ice loss cannot explain the rapid AA response. However, sea ice-related feedbacks do become important for AA after the first few months (even within the first year).

An important question that arises from our results is: To what extent does the rapid AA response—and its underlying physical mechanisms—depend on the climate state when the forcing is imposed? Recall that in our analysis, we examined the CMIP5 abrupt4×CO_2 simulations that were initialized from a preindustrial (piControl) climate state (see section 2.1). Furthermore, these simulations were initialized during the month of January, which is polar night at high northern latitudes. Thus, the models' climate state in the Arctic when CO_2 was instantaneously quadrupled was characterized by a strong near-surface inversion, extensive sea ice cover, and an absence of insolation. The latter implies a negligible contribution from Arctic shortwave feedbacks (e.g., surface albedo feedback) to the rapid Arctic warming occurring in the first few months of the simulations (see Figure 4a). Future work should investigate the climate state dependence of the rapid AA response identified here, for instance, by examining abrupt4×CO_2 simulations initialized at other times of the year.

Finally, in addition to providing insight into the physical causes of AA, our work also has important practical implications. Specifically, the inherently fast timescales of AA suggest the potential for near-term mitigation of Arctic warming following a reduction in anthropogenic forcing. We stress that this should not be taken as license to delay mitigation efforts, since prolonged delay could result in the passing of tipping points (Lenton, 2012) that would make large and deleterious climate change unavoidable. Our results provide a

sense of optimism though that the present trajectory of Arctic change can be altered on societally relevant timescales through swift action to limit greenhouse gas emissions.

Data Availability Statement

All CMIP5 data in the analysis are available for download online (https://esgf-node.llnl.gov/projects/cmip5/). Users should click on "Search for CMIP5 project data" and then select the appropriate search criteria: project (CMIP5), model (see section 2.1 for specific models analyzed), experiment (abrupt4×CO_2 or piControl), time frequency (mon), realm (atmos, ocean, or seaIce), ensemble (r1i1p1), and variable long name (see section 2.1 for specific variables analyzed). Code is available online (https://github.com/tyfolino/CMIP5_Arctic_Amplification and https://doi.org/10.5281/zenodo.3994734).

Acknowledgments

We thank two anonymous reviewers whose comments improved the manuscript. We acknowledge the World Climate Research Programme's Working Group on Coupled Modelling, which is responsible for CMIP, and we thank the climate modeling groups for producing and making available their model output. This work was supported by a grant from the National Science Foundation to Columbia University (Award 1603350). G. C. is funded by the Swiss National Science Foundation (Schweizerischer Nationalfonds zur Förderung der Wissenschaftlichen Forschung [SNSF]) Ambizione Grant PZ00P2-180043.

References

Bintanja, R., & van der Linden, E. C. (2013). The changing seasonal climate in the Arctic. *Scientific Reports*, *3*(1), 1556. https://doi.org/10.1038/srep01556

Bintanja, R., van der Linden, E. C., & Hazeleger, W. (2012). Boundary layer stability and Arctic climate change: A feedback study using EC-Earth. *Climate Dynamics*, *39*(11), 2659–2673. https://doi.org/10.1007/s00382-011-1272-1

Boeke, R. C., & Taylor, P. C. (2018). Seasonal energy exchange in sea ice retreat regions contributes to differences in projected Arctic warming. *Nature Communications*, *9*(1), 5017. https://doi.org/10.1038/s41467-018-07061-9

Cai, M. (2005). Dynamical amplification of polar warming. *Geophysical Research Letters*, *32*, L22710. https://doi.org/10.1029/2005GL024481

Carton, J. A., Chepurin, G. A., & Chen, L. (2018). SODA3: A new ocean climate reanalysis. *Journal of Climate*, *31*(17), 6967–6983. https://doi.org/10.1175/JCLI-D-18-0149.1

Conley, A., Lamarque, J. F., Vitt, F., Collins, W., & Kiehl, J. (2013). PORT, a CESM tool for the diagnosis of radiative forcing. *Geoscientific Model Development*, *6*(2), 469–476. https://doi.org/10.5194/gmd-6-469-2013

Dai, A., Luo, D., Song, M., & Liu, J. (2019). Arctic amplification is caused by sea-ice loss under increasing CO_2. *Nature Communications*, *10*(1), 121. https://doi.org/10.1038/s41467-018-07954-9

Fels, S., Mahlman, J., Schwarzkopf, M., & Sinclair, R. (1980). Stratospheric sensitivity to perturbations in ozone and carbon dioxide: Radiative and dynamical response. *Journal of the Atmospheric Sciences*, *37*(10), 2265–2297. https://doi.org/10.1175/1520-0469(1980)037<2265:SSTPIO>2.0.CO;2

Goosse, H., Kay, J. E., Armour, K. C., Bodas-Salcedo, A., Chepfer, H., Docquier, D., et al. (2018). Quantifying climate feedbacks in polar regions. *Nature communications*, *9*, 1919.

Graversen, R. G., & Langen, P. L. (2019). On the role of the atmospheric energy transport in 2 × CO_2-induced polar amplification in CESM1. *Journal of Climate*, *32*(13), 3941–3956. https://doi.org/10.1175/JCLI-D-18-0546.1

Hall, A. (2004). The role of surface albedo feedback in climate. *Journal of Climate*, *17*(7), 1550–1568. https://doi.org/10.1175/1520-0442(2004)017<1550:TROSAF>2.0.CO;2

Hansen, J., Sato, M., Kharecha, P., & von Schuckmann, K. (2011). Earth's energy imbalance and implications. *Atmospheric Chemistry and Physics*, *11*(24), 13,421–13,449. https://doi.org/10.5194/acp-11-13421-2011

Hansen, J., Sato, M., & Ruedy, R. (1997). Radiative forcing and climate response. *Journal of Geophysical Research*, *102*(D6), 6831–6864. https://doi.org/10.1029/96JD03436

Hwang, Y.-T., Frierson, D. M. W., & Kay, J. E. (2011). Coupling between Arctic feedbacks and changes in poleward energy transport. *Geophysical Research Letters*, *38*, L17704. https://doi.org/10.1029/2011GL048546

Kim, K.-Y., Hamlington, B. D., Na, H., & Kim, J. (2016). Mechanism of seasonal Arctic sea ice evolution and Arctic amplification. *The Cryosphere*, *10*(5), 2191–2202. https://doi.org/10.5194/tc-10-2191-2016

Lenton, T. M. (2012). Arctic climate tipping points. *Ambio*, *41*(1), 10–22. https://doi.org/10.1007/s13280-011-0221-x

Lu, J., & Cai, M. (2009). Seasonality of polar surface warming amplification in climate simulations. *Geophysical Research Letters*, *36*, L16704. https://doi.org/10.1029/2009GL040133

Manabe, S., & Stouffer, R. J. (1980). Sensitivity of a global climate model to an increase of CO_2 concentration in the atmosphere. *Journal of Geophysical Research*, *85*(C10), 5529–5554. https://doi.org/10.1029/JC085iC10p05529

Manabe, S., & Wetherald, R. T. (1975). The effects of doubling the CO_2 concentration on the climate of a general circulation model. *Journal of the Atmospheric Sciences*, *32*(1), 3–15. https://doi.org/10.1175/1520-0469(1975)032<0003:TEODTC>2.0.CO;2

Marshall, J., Scott, J. R., Armour, K. C., Campin, J. M., Kelley, M., & Romanou, A. (2015). The ocean's role in the transient response of climate to abrupt greenhouse gas forcing. *Climate Dynamics*, *44*, 2287–2299.

Merlis, T. M. (2015). Direct weakening of tropical circulations from masked CO_2 radiative forcing. *Proceedings of the National Academy of Sciences USA*, *112*(43), 13,167–13,171. https://doi.org/10.1073/pnas.1508268112

Osborne, E., Richter-Menge, J. & Jeffries, M. (Eds.) (2018). "Arctic report card 2018", https://www.arctic.noaa.gov/Report-Card

Pendergrass, A. G., Conley, A., & Vitt, F. M. (2018). Surface and top-of-atmosphere radiative feedback kernels for CESM-CAM5. *Earth System Science Data*, *10*(1), 317–324. https://doi.org/10.5194/essd-10-317-2018

Pithan, F., & Mauritsen, T. (2014). Arctic amplification dominated by temperature feedbacks in contemporary climate models. *Nature Geoscience*, *7*(3), 181–184. https://doi.org/10.1038/ngeo2071

Ramanathan, V., & Dickinson, R. E. (1979). The role of stratospheric ozone in the zonal and seasonal radiative energy balance of the earth-troposphere system. *Journal of the Atmospheric Sciences*, *36*, 1084–1104.

Screen, J. A., & Simmonds, I. (2010a). Increasing fall-winter energy loss from the Arctic Ocean and its role in Arctic temperature amplification. *Geophysical Research Letters*, *37*, L16707. https://doi.org/10.1029/2010GL044136

Screen, J. A., & Simmonds, I. (2010b). The central role of diminishing sea ice in recent Arctic temperature amplification. *Nature*, *464*(7293), 1334–1337. https://doi.org/10.1038/nature09051

Serreze, M. C., Barrett, A. P., Stroeve, J. C., Kindig, D. N., & Holland, M. M. (2009). The emergence of surface-based Arctic amplification. *The Cryosphere*, *3*(1), 11–19. https://doi.org/10.5194/tc-3-11-2009

Singh, H. A., Rasch, P. J., & Rose, B. E. J. (2017). Increased ocean heat convergence into the high latitudes with CO_2 doubling enhances polar-amplified warming. *Geophysical Research Letters*, *44*, 10,583–10,591. https://doi.org/10.1002/2017GL074561

Smith, K. L., Chiodo, G., Previdi, M., & Polvani, L. M. (2018). No surface cooling over Antarctica from the negative greenhouse effect associated with instantaneous quadrupling of CO_2 concentrations. *Journal of Climate*, *31*(1), 317–323. https://doi.org/10.1175/JCLI-D-17-0418.1

"Snow, Water, Ice and Permafrost in the Arctic (SWIPA) (2017)." Arctic Monitoring and Assessment Programme (2017).

Soden, B. J., Held, I. M., Colman, R., Shell, K. M., Kiehl, J. T., & Shields, C. A. (2008). Quantifying climate feedbacks using radiative kernels. *Journal of Climate*, *21*(14), 3504–3520. https://doi.org/10.1175/2007JCLI2110.1

Stocker, T. F., Qin, D., Plattner, G.-K., Tignor, M., Allen, S. K., Boschung, J., et al. (2013). "Climate change: The physical science basis. Contribution of Working Group I to the Fifth Assessment Report of the Intergovernmental Panel on Climate Change" (Cambridge University Press, 2013).

Taylor, K. E., Stouffer, R. J., & Meehl, G. A. (2012). An overview of CMIP5 and the experiment design. *Bulletin of the American Meteorological Society*, *90*, 485–498.

Wang, Y., & Huang, Y. (2020). Understanding the atmospheric temperature adjustment to CO_2 perturbation at the process level. *Journal of Climate*, *33*(3), 787–803. https://doi.org/10.1175/JCLI-D-19-0032.1

Zhang, M., & Huang, Y. (2014). Radiative forcing of quadrupling CO_2. *Journal of Climate*, *27*(7), 2496–2508. https://doi.org/10.1175/JCLI-D-13-00535.1